

Fluid-structure interaction in abdominal aortic aneurysms: structural and geometrical considerations

Yaser Mesri^{*,†}, Hamid Niazmand^{*,†,§}, Amin Deyranlou^{*,†}
and Mahmood Reza Sadeghi[‡]

**Department of Mechanical Engineering
Ferdowsi University of Mashhad, Mashhad, Iran*

*†Research Center for Biomedical Engineering
Ferdowsi University of Mashhad, Mashhad, Iran*

*‡Department of Biomedical Engineering
University of Isfahan, Isfahan, Iran*

§niazmand@um.ac.ir

Received 15 June 2014

Accepted 28 July 2014

Published 28 August 2014

Rupture of the abdominal aortic aneurysm (AAA) is the result of the relatively complex interaction of blood hemodynamics and material behavior of arterial walls. In the present study, the cumulative effects of physiological parameters such as the directional growth, arterial wall properties (isotropy and anisotropy), iliac bifurcation and arterial wall thickness on prediction of wall stress in fully coupled fluid-structure interaction (FSI) analysis of five idealized AAA models have been investigated. In particular, the numerical model considers the heterogeneity of arterial wall and the iliac bifurcation, which allows the study of the geometric asymmetry due to the growth of the aneurysm into different directions. Results demonstrate that the blood pulsatile nature is responsible for emerging a time-dependent recirculation zone inside the aneurysm, which directly affects the stress distribution in aneurysmal wall. Therefore, aneurysm deviation from the arterial axis, especially, in the lateral direction increases the wall stress in a relatively nonlinear fashion. Among the models analyzed in this investigation, the anisotropic material model that considers the wall thickness variations, greatly affects the wall stress values, while the stress distributions are less affected as compared to the uniform wall thickness models. In this regard, it is confirmed that wall stress predictions are more influenced by the appropriate structural model than the geometrical considerations such as the level of asymmetry and its curvature, growth direction and its extent.

Keywords: Abdominal aortic aneurysm; peak wall stress; fluid-structure interaction; asymmetry; material model; wall thickness.

1. Introduction

Abdominal aortic aneurysm (AAA) is one of the most important vascular diseases that is characterized by a 50% increase in the diameter of a part of aorta that is located between the renal arteries and the iliac bifurcation.¹ Studies have shown that

in addition to genetic factors, several mechanical factors affect the appearance and progression of aneurysms including flow regime,² vessel geometry, and mechanical properties of the arterial wall.³ Aneurysm is caused by destruction of elastin and growth and deformation of collagen in the arterial wall leading to a decrease in elasticity of the aneurismal wall.⁴

Commonly, the risk of rupture in AAAs is determined based on the maximum diameter of the case. Aneurysm diameter of about 5.5 cm is a candidate for surgical treatment.^{5,6} However, recent investigations have doubted the adequacy of this criterion, since there have been reports of AAAs ruptures with diameters of less than 5.5 cm,⁷⁻⁹ especially in women.¹⁰

The most important factor among mechanical factors associated with the rupture of the AAA is wall stress that is often measured as the von Mises stress (σ_{VM}) acting on the arterial wall.^{4,11} From biomechanical point of view, rupture of an aneurysm occurs, when the stress from physiological environment exceeds the patient's arterial wall strength. It is believed that the strength of the aneurismal wall is specific for each patient, yet, Raghavan *et al.*¹² reported that the failure stress of AAA-specimens can vary regionally from 33.6 to 235.1 N/cm².

Primary numerical models of AAA have focused on computational solid stress (CSS) predictions with applying a static luminal pressure.^{4,13-15} Fillinger *et al.*¹⁶ with the help of CSS method have shown that stress analysis for predicting the rupture risk is 12% more accurate than using a measure based on the maximum diameter.

In search for stress-based predictions, several computational simulations of the AAA employing more realistic materials, geometries and flow conditions have been developed that consider the fluid-structure interactions.

Wolters *et al.*¹⁷ performed an early FSI simulation with some simplifications such as uniform wall thickness and an isotropic material model proposed by Raghavan and Vorp (R&V model).¹⁸ Humphrey and Taylor¹⁹ confirmed that FSI simulations with appropriate boundary conditions are more useful for the aneurismal studies.

An interesting investigation on biomechanics of AAAs is the FSI study proposed by Scotti *et al.*¹³ with the help of an idealized geometry and a realistic approximate variable wall thickness. They demonstrated that the asymmetry and variable wall thickness of the pathological aorta lead to higher mechanical stresses and an increased risk of rupture as compared to the uniform wall assumption.

Rodriguez *et al.*³ also examined the influence of asymmetry and material anisotropy, yet, they continued the linear elastic FEA method for simulations of AAAs with the assumption of uniform wall thickness.

Rissland *et al.*²⁰ performed the recent FSI study using the anisotropic wall material in patient-specific models with a uniform wall thickness. They also presented a comparison of the wall stress between two isotropic and anisotropic material models.

Recent FSI works are performed on other characteristics of AAAs. Wang *et al.*²¹ investigated the effects of varying blood viscosity on stress predictions. Influence of intraluminal thrombus (ILT) in a realistic model of AAA with a Mooney–Rivlin

(MR) model has been studied by Polzer *et al.*²² Reymond *et al.*²³ have studied the impact of surrounding tissue of aorta wall on predictions of stress and wall displacement.

In the review paper of Humphrey and Holzapfel,¹¹ the most recent FSI studies are very well reviewed and categorized in a table format, which indicates that in most AAA studies a uniform wall thickness is considered.

In a more recent attempt to investigate the AAAs rupture risk, Scotti *et al.*²⁴ extended their previous study of the idealized geometrical model with considering the environmental pressure and more complicated boundary conditions. Again, they confirmed that variable wall thickness predicts higher stresses and rupture risk as compared to the models experiencing a constant wall thickness. They considered the aneurysm far enough from the iliac bifurcation and therefore, the effects of presence of the iliac bifurcation on the assessment of rupture risks were not examined. Nevertheless, Deplano *et al.*²⁵ experimentally examined the effects of the presence of iliac bifurcation on flow dynamics of an idealized AAA model. It was found that the presence of bifurcation strongly affected the AAA sac vortex intensities, which directly influenced the wall stress distributions.

In the present investigation, fully coupled FSI simulations of three-dimensional idealized geometrical models of AAA with considering the iliac bifurcation are presented. To the authors' knowledge, this work also represents the first fully coupled FSI model of an idealized AAA with an iliac bifurcation, which allows the study of the geometric asymmetry due to the growth of the aneurysm into different directions. Present study represents a comparison between an isotropic MR and a new anisotropic orthotropic material model via considering uniform wall thickness. Furthermore, the developed numerical model is capable to examine the effects of heterogeneity of arterial wall thickness in prediction the risk of rupture.

2. Aneurismal Geometry

The CAD software Solidworks is used to create five geometrical models with different directions of aneurismal growth as shown in Fig. 1. In Fig. 2, detailed specifications of AAA model for the case of $A_Y = 2$ in Fig. 1 are given as partially provided by Ref. 26. Other geometrical models can be easily built based on Fig. 2 data and specifications of the directional growth of aneurysm as will be discussed below. Inlet, outlet and aneurysm diameters are 3, 2 and 6 cm respectively, for a 14 cm arterial length. Following Scotti *et al.*²⁴ 1.5 mm wall thickness is considered for uniform aneurismal wall cases. Growth of aneurysms can occur in any directions from the anterior wall because of the existence of vertebral column in the posterior side, which prevents the aneurismal growth in this direction. In this study, aneurismal growth normal to the anterior wall (along the Y -axis) and the lateral wall (along the X -axis) are considered. Aneurismal growth in each direction is described by the parameter A defined as $A = R/r$, where R and r are distances of aneurysm dome and posterior side from the arterial axis, respectively as shown in Fig. 1.

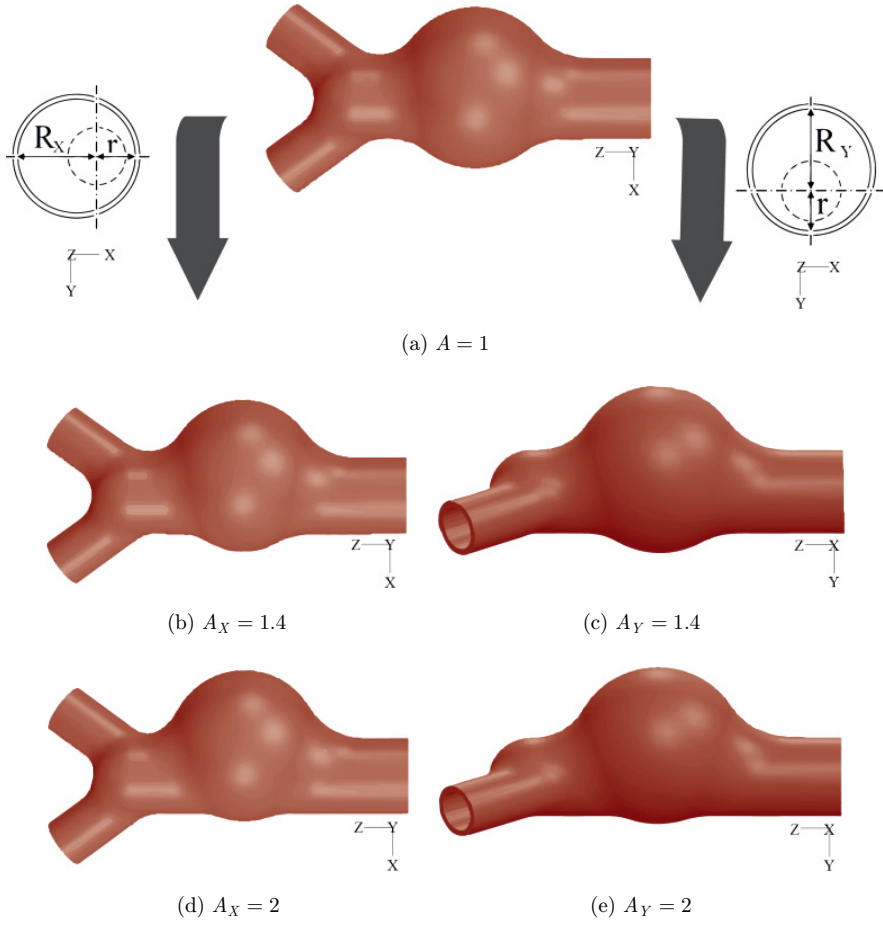


Fig. 1. (Color online) Different aneurismal geometries. Each model includes a fluid and a solid domain.

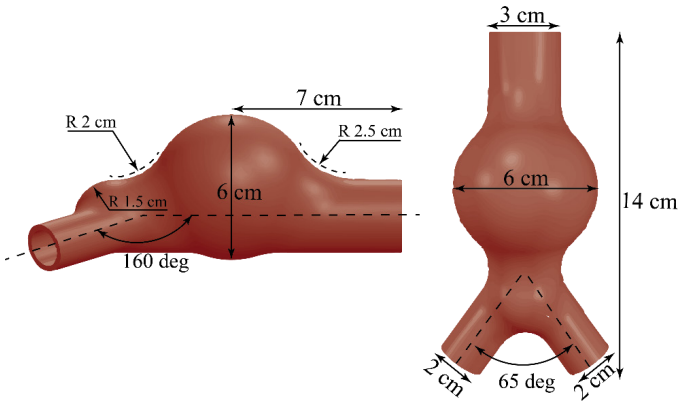


Fig. 2. (Color online) Geometrical specifications of the model with $A_Y = 2$.

3. Governing Equations and Boundary Conditions

Governing equations are the Navier–Stokes equations for a laminar, incompressible and Newtonian flow, due to the relatively high flow rate in aorta and its branches.^{27,28} Momentum equations in the Arbitrary Lagrangian–Eulerian (ALE) form for the fluid domain are expressed as:

$$\rho_f \frac{\partial v}{\partial t} + \rho_f ((v - w) \cdot \nabla)v - \nabla \cdot \tau_f = 0, \quad (1)$$

where w is the moving mesh velocity vector, ρ_f is the fluid density and v is the velocity vector. The fluid stress tensor (τ_f) is:

$$\tau_f = -p\delta_{ij} + 2\mu\varepsilon_{ij}, \quad (2)$$

where the strain rate (ε_{ij}) is defined as follows:

$$\varepsilon_{ij} = \frac{1}{2}(\nabla v + \nabla v^T), \quad (3)$$

where p is the fluid pressure, δ_{ij} is Kronecker delta and μ is the fluid viscosity. Blood density and viscosity are taken as $\rho_f = 1050 \text{ kg/m}^3$ and $\mu = 3.5 \text{ cP}$, respectively.²⁹

For the solid arterial wall, the Lagrangian coordinate is used, where the material particles are followed by a moving coordinate system. The solid elastodynamics momentum equation can be expressed as:

$$\nabla \cdot \tau_s + f_s^B = \rho_s \ddot{d}_s, \quad (4)$$

where τ_s is the solid stress tensor, f_s^B is the body force per unit volume, $\rho_s = 1200 \text{ kg/m}^3$ is the density of arterial wall and \ddot{d}_s is its local acceleration.

Two different models are used to describe the wall behavior. In the first model, a nonlinear, isotropic and hyperelastic material with a simplified model of the strain energy density function, which is described as MR material model is considered.

$$\Psi = \alpha(I_1 - 3) + \gamma(I_1 - 3)^2, \quad (5)$$

where Ψ is the strain energy, I_1 , is the first invariant of the left Cauchy–Green tensor and the values of $\alpha = 17.4 \text{ N/cm}^2$ and $\gamma = 188.1 \text{ N/cm}^2$ are based on the experimental data.¹⁸

In the second material model, Rissland *et al.*²⁰ adapted the exponential strain energy material model proposed by Vito and Hickey³⁰ to FSI modeling, by implementation of the orthotropic material model which is developed by Holzapfel *et al.*³¹ for multilayer arterial walls. The tissue is considered as a fiber-reinforced composite material with the fibers corresponding to the collagenous component of the material. The strain energy function for AAA wall is given by:

$$\Psi = \Psi_{\text{iso}} + \Psi_{\text{aniso}}, \quad (6)$$

$$\Psi_{\text{iso}} = C_1(I_1 - 3) + C_2(I_1 - 3)^2 + D_1(\exp\{D_2(I_1 - 3)\} - 1), \quad (7)$$

Table 1. Values of the material parameters for the anisotropic model.

Parameter	C_1 [kPa]	C_2 [kPa]	D_1 [kPa]	D_2	k_1 [kPa]	k_2	β_a [deg]	β_b [deg]
Value	8.888	164.9	0.0487	53.46	1.886	94.75	5	265

$$\Psi_{\text{aniso}} = \frac{k_1}{2k_2} \sum_{i=4,6} (\exp\{k_2(J_i - 1)^2\} - 1), \quad (8)$$

where

$$J_4 = C_{ij}(n_a)_i(n_b)_j, \quad J_6 = C_{ij}(n_a)_j(n_b)_i, \quad (9)$$

where C_{ij} is the Cauchy–Green deformation tensor, n_a and n_b are directions of the fiber defined by angles β_a and β_b , which are the offsets from the material axes. The related data taken from Ref. 20 are listed in Table 1.

For boundary conditions, a time-dependent velocity profile with time averaged Reynolds number of 410 at the inlet is applied, while a time-dependent pressure profile is considered at the outlet as a normal traction. The velocity and pressure waveforms are extracted from Doppler ultrasound for AAAs.³² As shown in Fig. 3, peak systolic flow and pressure occur at $t/T = 0.5$ and 0.55 , respectively, where T is the heart beat period. Womersley number, which characterizes the flow geometry, frequency and fluid viscous properties is set to $\alpha = 22.2$.³³

The geometry is fixed at the inlet and outlet, which are far enough from the AAA sac, and therefore, the AAA sac displacement is slightly influenced by this limitation. Because the arterial wall is surrounded by tissues and organs, an external pressure of 12 mmHg is applied on the outer surface of the arterial wall.³⁴

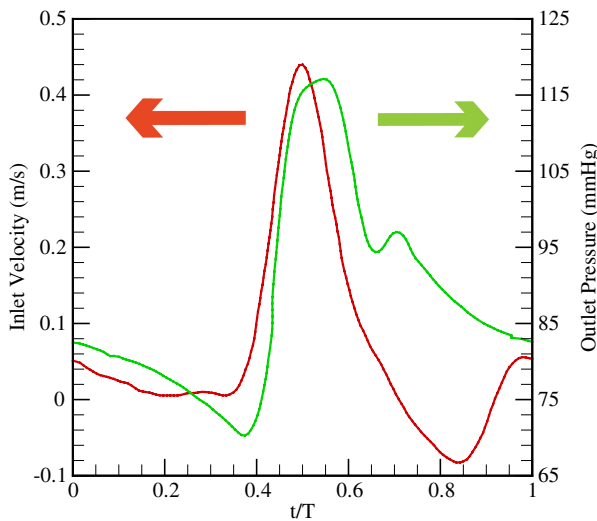


Fig. 3. (Color online) The pulsatile velocity and pressure waveforms reproduced from Ref. 32.

For fluid-structure interface conditions, it is assumed that displacements and surface forces are identical for both domains, and fluid domain follows the no-slip condition at wall interface, which are expressed as:

$$d_F = d_S, \quad (10)$$

$$n \cdot \sigma_F = n \cdot \sigma_S, \quad (11)$$

$$\dot{d}_F = \dot{d}_S, \quad (12)$$

where d is the displacement, σ is the stress tensor, n is the normal direction to the boundary surface and subscripts F and S denote the fluid and solid domains, respectively.

4. Numerical Modeling

The fully coupled equations of the fluid and solid domains are solved by the ADINA software package (v8.5, ADINA R&D, Inc., Watertown, MA), which is well-known in the area of blood hemodynamics and fluid-structure interaction.^{13,20,24}

The employed direct coupling method combines the solid and fluid matrices during the solution process. The second-order upwind method and the backward Euler method are used for spatial and time integrations, respectively. Newton–Raphson method is used for linearization process. Four node linear tetrahedral elements are used for discretization of both fluid and solid domains. A sparse matrix solver based on the Gaussian elimination method is used in the solution process. The relative tolerance for all degrees of freedom is set to 0.001. The periodic time convergence for the displacement and wall stress of the fluid–solid interface is usually achieved within six cardiac cycles. Simulations were performed on the Intel®Core™i7-3770kCPU@3.50-3.90 GHz and 32GB (RAM). The simulation time for one cardiac cycle was approximately 44 CPU-hours.

5. Model Validation

To verify the grid independence, numerical simulations are reported for geometrical model of $A_Y = 2$ with 21 567, 41 934, 50 310, 58 725 and 69 546 tetrahedral elements for the solid domain, and 167 437, 240 944, 298 043, 340 981 tetrahedral elements for the fluid domain. Different sets of solid and fluid domain elements including 20 simulations are considered to identify that the final set of 44 372 and 329 671 grid elements in solid and fluid domains, respectively, are adequate for producing grid independent results. As a typical result, in Fig. 4 the variations of the maximum wall stress for three monitoring points at the time of peak systolic velocity are presented for varying fluid elements, while the solid domain elements are kept at 44 372. Between the last two finer grids, the results are almost similar, therefore, an intermediate grid with 329 671 tetrahedral elements is chosen for fluid domain. For other fluid and solid models, similar procedures have been carried out and grid independent results are reported.

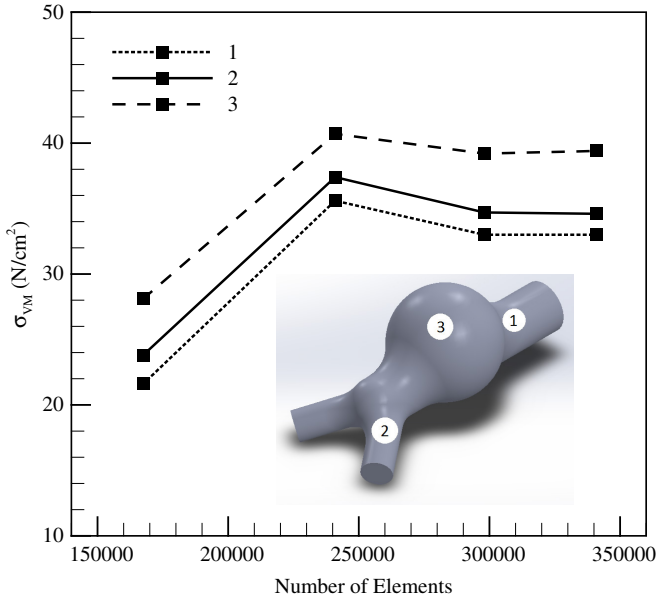


Fig. 4. Stress variations with respect to the number of grid elements for three monitoring points of fluid domain at the interface boundary with the solid domain.

Typical tetrahedral elements distribution in the fluid domain of $A_Y = 2$ model is shown in Fig. 5.

We validated our numerical results against the numerical results of Tezduyar *et al.*²⁶ for a relatively similar $A_Y = 2$ model with uniform wall thickness of 2.3 mm. A linear elastic material model along with a pulsatile inflow velocity profile with minimum and maximum values of 0.13 m/s and 1.13 m/s is employed. All other

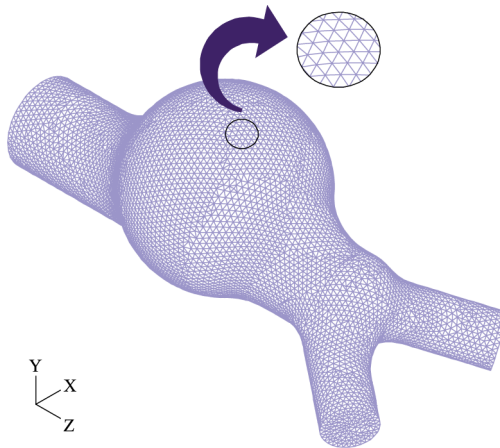


Fig. 5. (Color online) Tetrahedral elements distribution for the fluid domain of $A_Y = 2$ model.

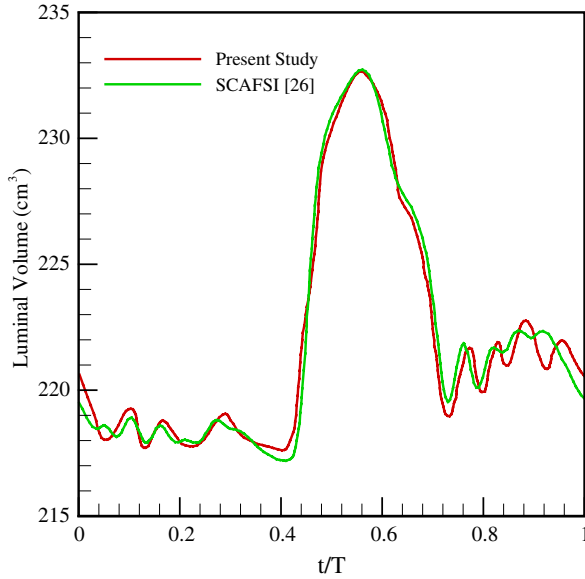


Fig. 6. (Color online) Comparison of the temporal variation of the luminal volume during one cycle time.

specifications can be found in Ref. 26. Unfortunately, very limited data are provided for comparison. Therefore, time variations of the luminal volume during one cycle time are compared in Fig. 6, where reasonable agreements are found. Slight discrepancies can be attributed to the possible differences in the reproduced AAA geometry model since some minor specifications were not provided. It is noteworthy that time variations of the luminal volume, adequately reflects the interaction between the fluid and solid domains, which is an important component for the accuracy of the calculations.

6. Results and Discussion

6.1. Solid dynamics

Figures 7(a)–7(d) show the temporal evolution of both maximum stress and displacement of the arterial wall for different aneurismal growths and material models during one cycle time. Figures 7(a) and 7(b) indicate that the peak wall stresses for all cases occur almost at $t/T = 0.52$. Considering Fig. 3, this point is corresponding to a point between the peak systolic flow and pressure, where both velocity and pressure are close to their maximum values. The local minimum at $t/T = 0.59$ is due to the abrupt drop in velocity magnitude, which also corresponds to the peak systolic pressure that leads to the ascending behavior of stress curves up to $t/T = 0.64$. Later on, the stress experiences a relatively strong drop due to the rapid decrease in pressure, which is also coincided with the lowest values of the inlet velocity profile.

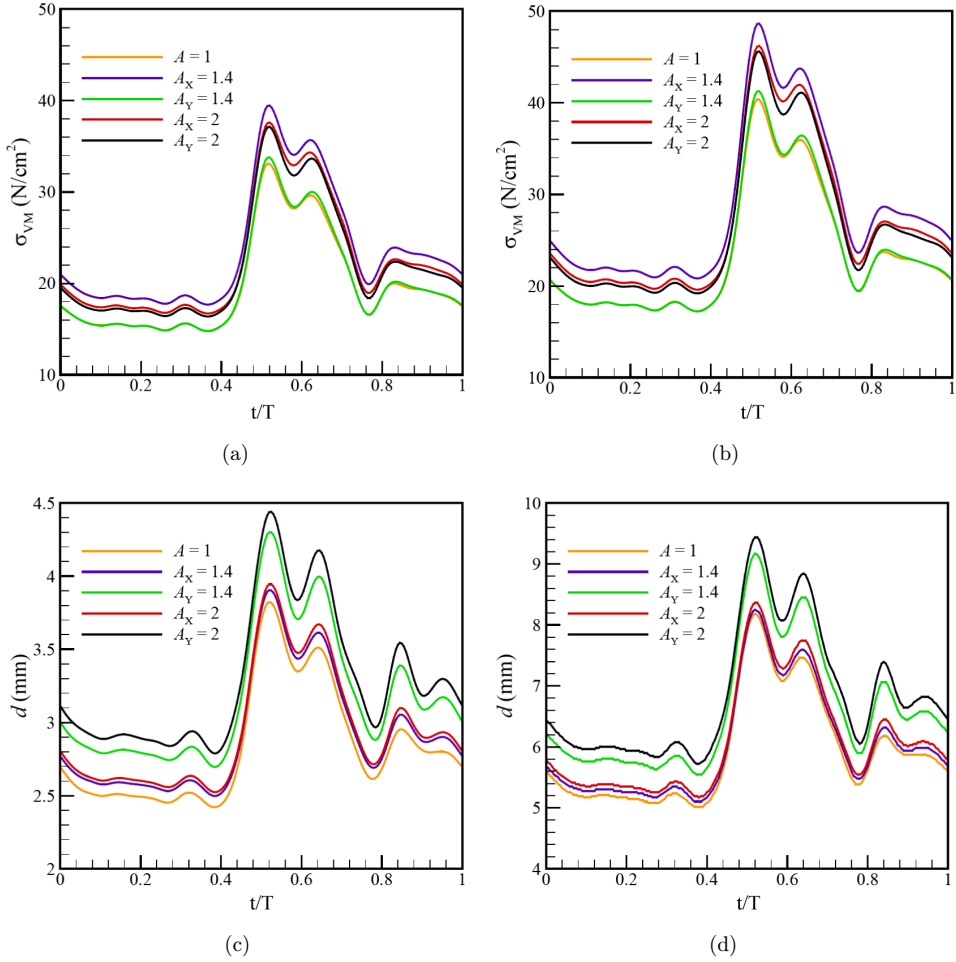


Fig. 7. (Color online) Temporal variations of the maximum wall stresses for; (a) isotropic, (b) anisotropic model; and wall displacements for; (c) isotropic, (d) anisotropic model, for different geometrical models.

Small fluctuations in stress curves for the rest of the cycle time are due to the interaction of the oscillations present in both velocity and pressure profiles. Comparing Fig. 7(a) with Fig. 7(b) shows that the anisotropic model predicts higher stresses of about 25% for aneurysmal growths than the MR model, yet, the temporal variations for both material models follows the same trend. Furthermore, for both material models, the aneurysmal growths in the lateral direction (X -axis) are associated with higher stresses as compared to the growths in the normal direction (Y -axis). It is also interesting to note that the aneurysmal growth of $A_X = 1.4$ in the lateral direction shows highest stresses among all cases, which will be discussed in more details when the dynamics of aneurysmal flows are considered in Fig. 9.

It is expected that the temporal variations of the maximum wall stresses be related with their corresponding maximum displacement variations of the arterial wall as indicated by Figs. 7(c) and 7(d). Again, similar trends in the temporal displacement variations for both materials and aneurismal growths are observed. However, anisotropic model predictions are about 110% higher than the MR model. In contrast to the temporal variations of the maximum stresses, which is highest for the lateral direction ($A_X = 1.4$), higher displacements occur for the growth in normal direction ($A_Y = 2$ and 1.4), which can be attributed to the circulating flows in the aneurysm as will be clarified with respect to Fig. 9.

Spatial outer surface distributions of wall stress for different aneurismal growths are presented for the anisotropic model in Fig. 8 corresponding to the peak maximum wall stress at $t/T = 0.52$ in Fig. 7(b). Note that for more clarity, same colors in different figures are not representing the same stress values. It is notable that the point of peak wall stress, which is identified by a Δ symbol in each figure, is located between the aneurysm dome and the iliac bifurcation for all geometrical models. Clearly, the high rupture risk regions do not coincide with the regions of maximum diameter in all cases.

6.2. Flow dynamics

Cross-sectional velocity vectors for various geometrical models of aneurysm with anisotropic wall are shown in Fig. 9 at the peak wall stress ($t/T = 0.52$) in coronal (XZ) and sagittal (YZ) planes in the aneurismal region. Velocity vectors are normalized with the corresponding maximum velocity value in the whole flow domain of each geometrical model.

Clearly, for the symmetrical aneurismal models with respect to the sagittal plane that are $A = 1$, $A_Y = 1.4$ and 2 , the core flow is in the arterial axis direction and relatively weaker circulating flows are observed in the aneurysm dome as compared to the A_X models. Figure 9(b) also shows that the strongest flow field exist for $A_X = 1.4$ model, which is in accordance with the largest peak stress time variations in Figs. 7(a) and 7(b). It is also notable that the order of the maximum velocity in different AAA models in Fig. 9 is consistent with the peak stress levels as shown in Figs. 7(a) and 7(b).

Comparing Fig. 9(b) with Fig. 9(d) indicates that for $A_X = 2$ the main core flow from the proximal remains attached to the left lateral wall directing a larger portion of the flow to the left branch of the iliac bifurcation. However, for the $A_X = 1.4$ model due to the larger curvature of the left lateral wall, the jet flow is separated from the wall and remains almost in the core area along the arterial axis leading to a more equal flow distribution in the iliac branches. This flow separation causes the formation of a stronger recirculation in the dome region of $A_X = 1.4$ model as compared to the $A_X = 2$ model, which also reflect in the peak stress distributions as mentioned earlier.

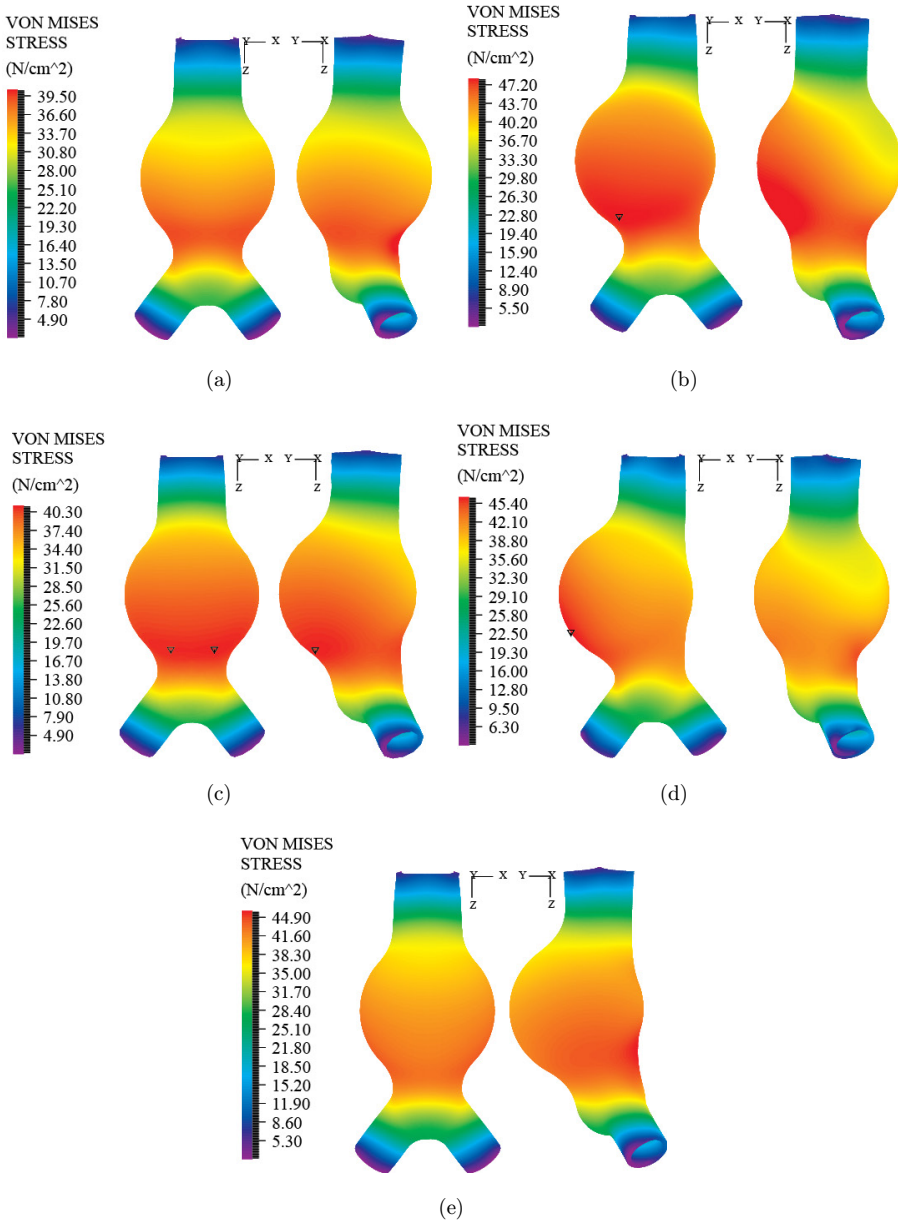


Fig. 8. (Color online) Comparison of outer wall stress distributions (at $t/T = 0.52$) for (a) $A = 1$, (b) $A_X = 1.4$, (c) $A_Y = 1.4$, (d) $A_X = 2$, (e) $A_Y = 2$. The symbol Δ indicates the location of peak wall stress.

Flow separations and creation of recirculation zones, especially for models with relatively weaker velocity patterns, cause longer residence times for flow particles within the AAA sac and increase the probability of formation and growth of a thrombus in the AAA sac.

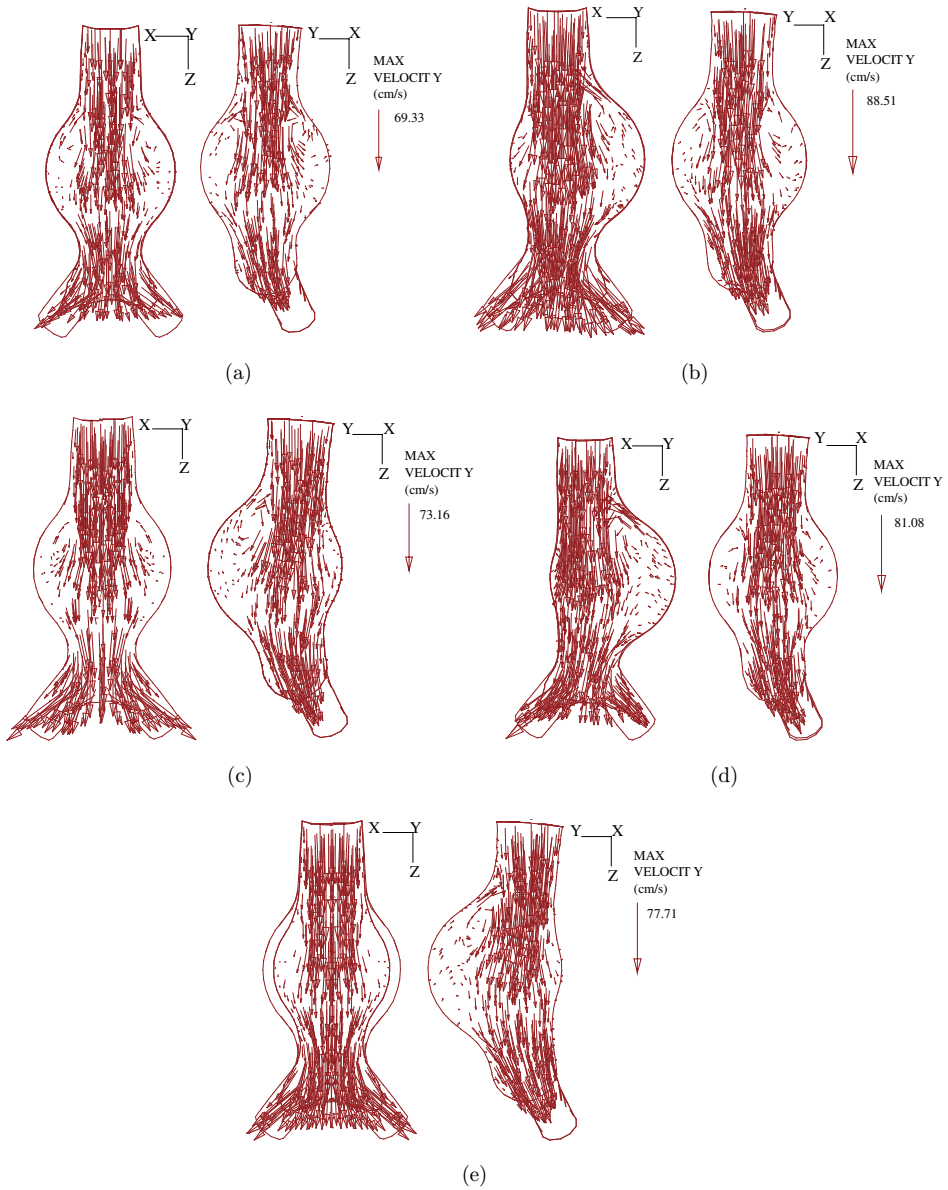


Fig. 9. (Color online) Velocity vectors at $t = 0.52$ for (a) $A = 1$, (b) $A_X = 1.4$, (c) $A_Y = 1.4$, (d) $A_X = 2$, (e) $A_Y = 2$. Vectors are normalized by the maximum velocity of each case.

7. Effects of Wall Thickness

Many attempts have been made to determine the extent of heterogeneity of the aneurysmal wall. Raghavan *et al.*¹² reported an average thickness of 1.5 mm for the aneurysmal wall. Because of the difficulty in obtaining the wall thickness from the CT

images, an averaged thickness of 1.5 mm is used in this study for cases with uniform wall thickness. From the biomechanical viewpoint, the wall thickness plays a significant role in the distribution of wall stress and is an important factor in assessing the risk of rupture in AAAs.

Stress predictions based on variable wall thickness have also been performed for all geometrical and material models previously considered for the uniform wall thickness at the same flow conditions. As mentioned above, it is not easy to determine the wall thickness from the CT images, therefore, in this study variable wall thickness is modeled based on the assumption of constant wall volume proposed by Scotti *et al.*¹³ In this relatively simple model, the wall thickness at each point varies according to its normal distance from the arterial centerline. Therefore, points with larger distances from the centerline are thinner in thickness. Based on this model, wall thickness varies between 0.5 mm and 1.5 mm for cases considered here.

The wall stress distributions for outer wall surface of variable wall thickness model, as shown in Fig. 10, present relatively similar patterns as compared to the uniform wall model shown in Fig. 8, and therefore, are presented just for $A_X = 1.4$ with anisotropic wall. Significant increase in wall stress distributions can be observed as compared to the uniform wall thickness in Fig. 8(b). Furthermore, the point of the maximum wall stress slightly moves toward the aneurysm dome, which is also true for other aneurysm geometries examined in the present study.

Similar to Fig. 7(b) for constant wall cases, the temporal variations of maximum wall stresses for anisotropic model with variable wall thickness for all aneurysmal growth directions are shown in Fig. 11. Again, anisotropic model for variable wall thickness predicts considerably higher values for wall stresses as compared to the uniform wall cases in Fig. 7(b), yet, the time variation trends for different geometrical models are similar.

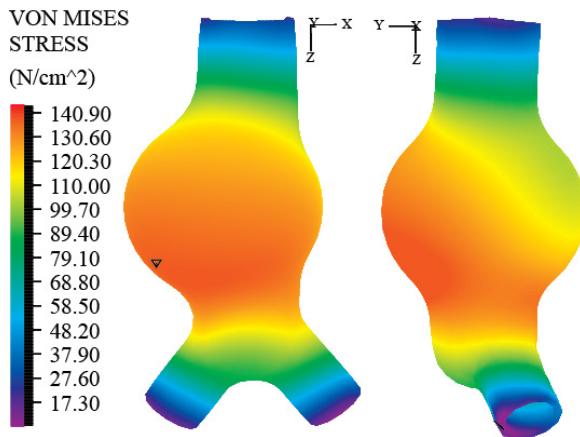


Fig. 10. (Color online) Outer wall stress distributions (at $t/T = 0.52$) for $A_X = 1.4$ with variable wall thickness.

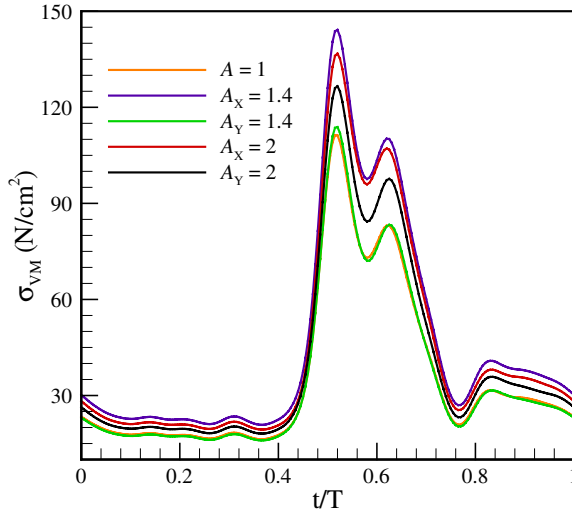


Fig. 11. (Color online) Temporal variations of maximum wall stresses for anisotropic model with variable wall thickness.

Figures 12 and 13 show the variations of the peak wall stresses with respect to the aneurysmal growth in one cardiac cycle for both uniform and variable wall thickness, respectively. The effect of material model is also included by comparison between the MR and anisotropic models.

Clearly, aneurysmal direction has significant effects on the peak stress variations. For aneurysmal growth in the normal direction there is a monotonic increase in peak stresses as parameter A increases, while in the lateral direction, increasing the A parameter enhances wall stress such that it reaches its maximum value in $A_X = 1.4$

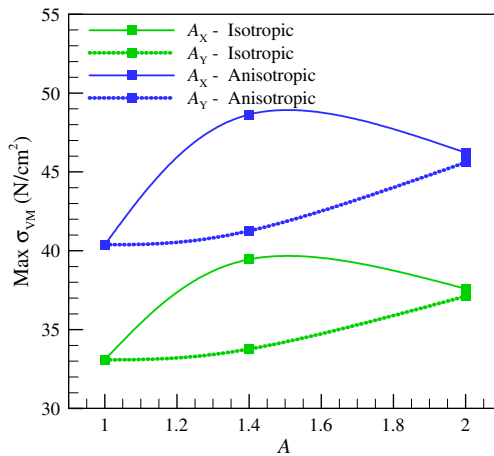


Fig. 12. (Color online) Peak wall stress for uniform wall thickness model in various aneurysmal growth and material models.

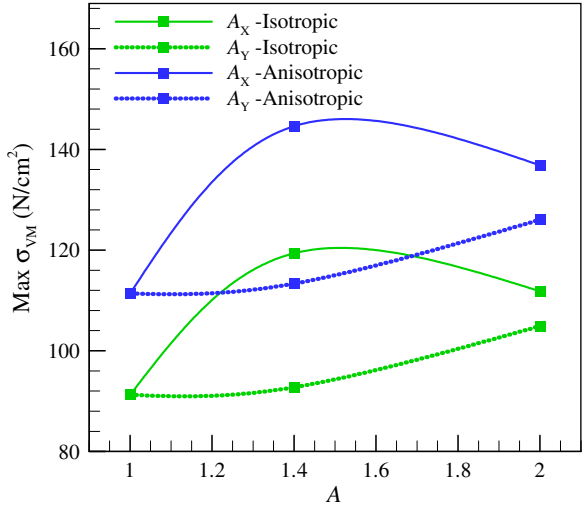


Fig. 13. (Color online) Peak wall stress for variable wall thickness model in various aneurismal growth and material models.

and reduces at larger values of A . Moreover, the stress values for A_X models are higher than A_Y models, owing to the stronger deviations of the geometry from the arterial axis and higher level of flow asymmetry.

Comparing Fig. 13 with Fig. 12 reveals that the maximum wall stress predictions with variable wall thickness model are approximately three times larger than those of uniform wall thickness for all geometrical models. This relatively significant increase indicates that the wall stresses are more influenced by the wall thickness model than the geometrical aspects of the aneurysm such as the level of asymmetry and its curvature, growth direction and its extent.

8. Conclusions

In the present study, we have investigated the effects of physiological parameters such as the directional growth, arterial wall properties, iliac bifurcation and the heterogeneity of arterial wall on predictions of wall stresses in a fully coupled FSI analysis of five idealized AAA models. Presence of iliac bifurcation allows examining the asymmetry effects of the growth of AAA sac into two different directions. Arterial wall is modeled with the commonly used isotropic MR model and the anisotropic orthotropic model. The effects of variable wall thickness are also examined and compared with the assumption of uniform wall thickness.

Results indicate that the peak wall stress increases by increasing the radial deviation of aneurysm from the arterial axis, which is more considerable for growth in lateral direction (along the X -axis) as compared to the normal direction (along the Y -axis). This confirms that presence of iliac bifurcation is essential in the stress analysis of the AAAs.

Implementation of variable wall thickness highly increases the values of wall stresses in both material models. The predictions of the anisotropic variable wall thickness model for maximum wall stresses are almost three times larger than those of uniform wall thickness models indicating the importance of the effects of variable wall thickness in comparison with the material models. Moreover, accurate structural models such as wall thickness and material models has more influence on wall stress predictions as compared to the geometrical aspects of the aneurysm such as the level of asymmetry and its curvature, growth direction and its extent.

Given the importance of the idealized geometries on presenting a general diagnostic tool to determine the need for surgery, the methodology presented here improves the previous efforts by considering more realistic and accurate parameters of physiological environment of AAAs.

Acknowledgment

This work was supported in part by the fund No. 3/28052 granted by the Ferdowsi University of Mashhad.

References

1. C. M. Crawford, K. Hurtgen-Grace, E. Talarico and J. Marley, *J. Manip. Physiol. Ther.* **26**, 184 (2003).
2. P. Blanco, I. Larrabide, R. Feijóo and S. Urquiza, Sensitivity of blood flow patterns to the constitutive law of the fluid, in *III European Conf. on Computational Mechanics*, eds. C. A. Motasoaes *et al.*, (Springer Netherlands, 2006), pp. 181–181.
3. J. F. Rodriguez, C. Ruiz, M. Doblare and G. A. Holzapfel, *J. Biomech. Eng.* **130**, 021 (2008).
4. D. A. Vorp, *J. Biomech.* **40**, 1887 (2007).
5. C. Fleming, E. P. Whitlock, T. L. Beil and F. A. Lederle, *Ann. Intern. Med.* **142**, 203 (2005).
6. F. A. Lederle *et al.*, *N Engl. J. Med.* **346**, 1437 (2002).
7. R. C. Darling, C. R. Messina, D. C. Brewster and L. W. Ottinger, *Circulation* **56**, 161 (1977).
8. L. C. Brown and J. T. Powell, *Ann. Surg.* **230**, 289 (1999).
9. J. L. Cronenwett *et al.*, *Surgery* **98**, 472 (1985).
10. T. L. Forbes, D. K. Lawlor, G. DeRose and K. A. Harris, *Ann. Vasc. Surg.* **20**, 564 (2006).
11. J. D. Humphrey and G. A. Holzapfel, *J. Biomech.* **45**, 805 (2012).
12. M. L. Raghavan, J. Kratzberg, E. M. Castro de Tolosa, M. M. Hanaoka, P. Walker and E. S. da Silva, *J. Biomech.* **39**, 3010 (2006).
13. C. Scotti, A. Shkolnik, S. Muluk and E. Finol, *BioMed. Eng. OnLine* **4**, 1 (2005).
14. E. S. Di Martino, A. Bohra, J. P. Vande Geest, N. Gupta, M. S. Makaroun and D. A. Vorp, *J. Vasc. Surg.* **43**, 570 (2006).
15. M. L. Raghavan, D. A. Vorp, M. P. Federle, M. S. Makaroun and M. W. Webster, *J. Vasc. Surg.* **31**, 760 (2000).
16. M. F. Fillinger, S. P. Marra, M. L. Raghavan and F. E. Kennedy, *J. Vasc. Surg.* **37**, 724 (2003).
17. B. J. Wolters, M. C. Rutten, G. W. Schurink, U. Kose, J. de Hart and F. N. van de Vosse, *Med. Eng. Phys.* **27**, 871 (2005).

18. M. L. Raghavan and D. A. Vorp, *J. Biomech.* **33**, 475 (2000).
19. J. D. Humphrey and C. A. Taylor, *Annu. Rev. Biomed. Eng.* **10**, 221 (2008).
20. P. Rissland, Y. Alemu, S. Einav, J. Ricotta and D. Bluestein, *J. Biomech. Eng.* **131**, 031001 (2009).
21. X. Wang and X. Li, *Comput. Biol. Med.* **41**, 812 (2011).
22. S. Polzer, T. C. Gasser, J. Swedenborg and J. Bursa, *Eur. J. Vasc. Endovasc. Surg.* **41**, 467 (2011).
23. P. Reymond, P. Crosetto, S. Deparis, A. Quarteroni and N. Stergiopoulos, *Med. Eng. Phys.* **35**, 784 (2013).
24. C. M. Scotti, J. Jimenez, S. C. Muluk and E. A. Finol, *Comput. Methods Biomech. Biomed. Eng.* **11**, 301 (2008).
25. V. Deplano, C. Meyer, C. Guivier-Curien and E. Bertrand, *Med. Eng. Phys.* **35**, 800 (2013).
26. T. E. Tezduyar, S. Sathe, M. Schwaab and B. S. Conklin, *Int. J. Numer. Methods Fluids* **57**, 601 (2008).
27. S. A. Berger and L.-D. Jou, *Annu. Rev. Fluid Mech.* **32**, 347 (2000).
28. C. M. Scotti and E. A. Finol, *Comput. Struct.* **85**, 1097 (2007).
29. E. A. Finol, K. Keyhani and C. H. Amon, *J. Biomech. Eng.* **125**, 207 (2003).
30. R. P. Vito and J. Hickey, *J. Biomech.* **13**, 951 (1980).
31. G. Holzapfel, T. Gasser and R. Ogden, *J. Elasticity Phys. Sci. Solids*, **61**, 1 (2000).
32. C. J. Mills et al., *Cardiovasc. Res.* **4**, 405 (1970).
33. W. Nichols, M. O'Rourke and C. Vlachopoulos, *McDonald's Blood Flow in Arteries, 16th edn. Theoretical, Experimental and Clinical Principles* (Taylor & Francis, 2011).
34. J. W. Hinnen, O. H. Koning, M. J. Visser and H. J. Van Bockel, *J. Vasc. Surg.* **42**, 1176 (2005).